Earth and Planetary Science Letters 276 (2008) 262–272

Contents lists available at ScienceDirect

Earth and Planetary Science Letters

journal homepage: www.elsevier.com/locate/epsl

Characteristic repeating earthquakes in an arc-continent collision boundary zone: The Chihshang fault of eastern Taiwan

Kate Huihsuan Chen [a,1], Robert M. Nadeau [b], Ruey-Juin Rau [a,*]

[a] Department of Earth Sciences, National Cheng Kung University, Tainan, 701, Taiwan, ROC
[b] Berkeley Seismological Laboratory, 211 McCone Hall, University of California, Berkeley, CA 94720-4760, USA

ARTICLE INFO

Article history:
Received 2 February 2007
Received in revised form 11 September 2008
Accepted 22 September 2008
Available online 8 November 2008

Editor: R.D. van der Hilst

Keywords:
repeating earthquake
creeping
Taiwan
cross-correlation coefficient
earthquake potential
arc-continent collision

ABSTRACT

Creeping crustal faults often generate a large number of microearthquakes, and less commonly, they may also produce major earthquakes that rupture the brittle crust. The Chihshang fault in eastern Taiwan is characterized by such behavior and has been known to undergo 2–3 cm/yr surface creep, making it one of the most active creeping thrust faults known in the world. It gives an excellent opportunity to study how a creeping fault can generate large earthquakes. However, the understanding of fault behavior at depth in this area has been limited due to sparse sampling from seismic and geodetic stations. In this study we determine and evaluate a population of repeating earthquakes to improve the understanding of deep fault deformation. We propose a repeating sequence identification scheme in the region where the station coverage is sparse and one-sided. Using this identification method, we found 30 M 2–3 characteristic repeating sequences under the northern half of the Chihshang fault at 7–23 km depth. Slip estimates from these sequences indicate an average slip rate of ~3 cm/yr, which is consistent with the rate inferred from surface geodetic measurements. We infer that the 30-km-long Chihshang fault is creeping along its northern half and locked in the south, consistent with the occurrence of the 2003 M_L 6.4 earthquake on the southern fault section.

1. Introduction

The Chihshang fault is located in the middle section of the Longitudinal Valley fault (LVF) system in eastern Taiwan. The 150-km-long, NNE trending LVF is a plate-suture boundary fault between the Eurasian continental margin and the Philippine Sea Plate (bold line in inset of Fig. 1), which accommodates 25–30% of the relative motion between the two plates (Barrier and Chu, 1984; Angelier et al., 2000; Yu and Kuo, 2001; Lee et al., 2001). During the past decades, the Chihshang fault has been documented as actively creeping based on progressive displacement of concrete retaining walls fractures in roads and buildings (e.g., Barrier and Chu, 1984; Chu et al., 1994; Lee, 1994; Angelier et al., 1997; Lee et al., 2001), and on rapid surface slip of about 2–3 cm/yr in the horizontal direction from GPS data (Yu and Kuo, 2001), which projects to ~4 cm/yr creep rate along the dip-slip direction. Continuously monitored creepmeters installed along the Chihshang fault from 1998 to 2001 indicate an annual shortening rate of 1.5–1.6 cm/yr, with higher shortening rates during the wet seasons and lower creep rates during dry seasons (Lee et al., 2003).

The most significant earthquakes that occurred on the Chihshang fault in historic times were a M_L 6.0 event in 1951 (Hsu, 1962; Cheng et al., 1996) and more recently a M_L 6.4 (M_w 6.5) earthquake on 10 December 2003. Because of these large earthquakes, this fault is considered to exhibit interseismic creep at the surface while also being capable of producing large earthquakes at depth. Aftershocks of the 2003 M_L 6.4 event were concentrated on the southern portion of the Chihshang fault and showed southward extension (Wu et al., 2006), suggesting that stress accumulation and release on the Chihshang fault may be strongly governed by spatial variations in fault zone properties at depth.

Earthquake relocation indicates that the Chihshang fault is a narrow SE-dipping inclined fault zone extending from the near surface to a depth of 25 km. Most of the earthquake activity on this fault occurs at depths between 12 and 23 km and is dominated by reverse-type focal mechanisms (Kuochen et al., 2004). Fault plane solutions for 1991–2003 M>3 earthquakes determined by P-wave polarities and SH/P amplitude ratios showed a dip angle of 40–50° between 10 and 20 km depth; the dip of the fault plane steepens upward (~70°) and flattens downward (~20°) (Chen and Rau, 2002). Geomorphic, geodetic, and structural data indicate that at the near surface, the Chihshang fault segment generally follows a major geological contact between the Pliocene Lichi Mélange to the east

Abbreviations: InSAR, Interferometric Synthetic Aperture Radar; LVF, Longitudinal Valley fault; CWBSN, Central Weather Bureau Seismic Network; ccc, cross-correlation coefficient; sps, samples per second; SNR, signal to noise ratio; dS_mP, differential S-P time; S_mP, S-P time; SVD, Singular Value Decomposition; tt_p, tt_s, P- and S- travel times; COV, coefficient of variation.

* Corresponding author. Tel.: +886 6 2757575 65425; fax: +886 6 2740285.
E-mail addresses: katepili@gmail.com (K.H. Chen), nadeau@seismo.berkeley.edu (R.M. Nadeau), raurj@mail.ncku.edu.tw (R.-J. Rau).
[1] Present address: Department of Earth Sciences, National Taiwan Normal University, No. 88, Sec. 4, Tingzhou Rd., Taipei 116, Taiwan, ROC.

0012-821X/$ – see front matter © 2008 Elsevier B.V. All rights reserved.
doi:10.1016/j.epsl.2008.09.021

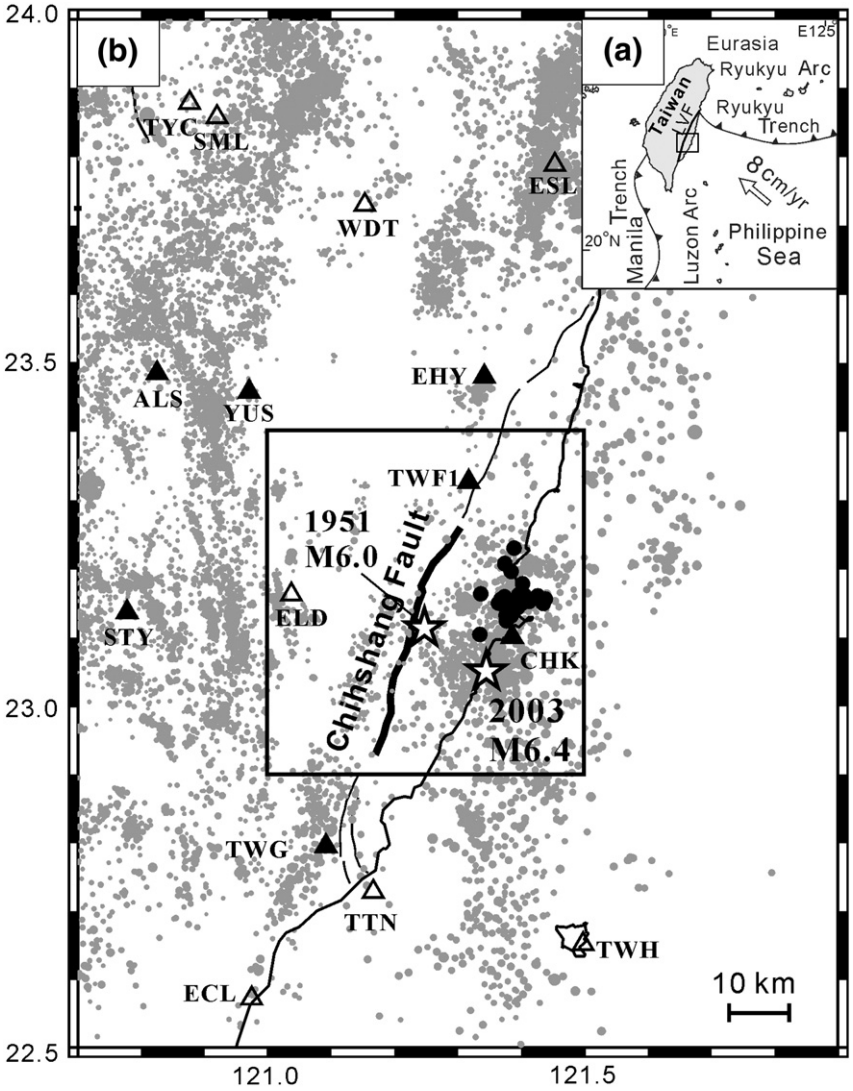

Fig. 1. (a) Geodynamic framework of Taiwan. Open arrow indicates relative motion between Philippine Sea plate and Eurasian plate in the Taiwan Region (Lee, 1994). The Longitudinal Valley fault (LVF) is considered to be the suture between these two plates. (b) The Chihshang fault segment and the Chihshang study area (box). HypoDD relocation of $M \geqq 3$ seismicity during the study period are shown as gray dots. The 7 seismic stations used in this study are shown as black triangles, others with relatively lower SNR are shown as open triangles. Locations of the 30 repeating sequences that we found are shown as black solid circles. Stars are the $M > 6$ historical earthquakes that occurred on the Chihshang fault.

(the Coastal Range) and the Pleistocene–Holocene deposits to the west (the Longitudinal Valley) (e.g., Lee et al., 2006). The weak recent deposits and the Mélange mudstones in the hanging wall of the Chihshang fault are likely to facilitate high rates of fault creep (Yu and Liu, 1989; Yu et al., 1997; Angelier et al., 2000; Yu and Kuo, 2001; Lee et al., 2001; Lee et al., 2003).

Faults that produce both large earthquakes and near surface creep have been studied on strike-slip faults (for example, the Hayward fault in central California) and are believed to consist of a combination of locked and creeping fault zones at depth (Savage and Lisowski, 1993; Bürgmann et al., 2000; Simpson, 2000). It is important to understand the distribution of locked and creeping fault zones at depth for earthquake potential assessment. However, due to limited geodetic coverage in this area, we lack well-resolved picture of fault slip rates at depth on the Chihshang fault. Interferometric Synthetic Aperture Radar (InSAR) data provides improved spatial sampling of the deformation field (e.g., Massonnet et al., 1993), but the nature of the landcover and atmospheric conditions in this area complicate the task of obtaining more detailed deformation information (Hsu and Bürgmann, 2006).

A new technique for inferring fault slip rate at depth using repeating microearthquakes was recently developed and has been applied in diverse tectonic settings (Nadeau and McEvilly, 1999; Bürgmann et al., 2000; Matsubara et al., 2005). Repeating earthquakes are defined as groups of events with nearly identical waveforms, locations, and magnitudes and thus represent a repeated rupture on the same fault patch (e.g., Poupinet et al., 1984; Ellsworth and Dietz, 1990; Vidale et al., 1994; Nadeau et al., 1995; Beroza et al., 1995). Given an assumption that the frequency of seismic slips on a fault patch is proportional to the tectonic loading rate due to relative plate motion, one can determine the deep fault slip rate at each repeating sequence site using the recurrence intervals and seismic moments of the repeating sequence (e.g., Nadeau and Johnson, 1998). A remarkably large number of small repeating earthquakes have been found in the creeping sections along the San Andreas fault due to a lower magnitude of completeness in the earthquake catalog with dense station coverage and high resolution data (e.g., Nadeau and McEvilly, 1999, 2004). In the creeping Chihshang area where spatial coverage of stations is sparse and asymmetric around the fault, however, repeating earthquake identification is problematic and challenging.

With a major limitation in searching for repeating earthquakes that could help resolve the distribution of fault creep at depth, we propose a relatively objective method called composite selection criteria to identify repeating events in this particular region.

Furthermore, we use these results to characterize repeating earthquake behavior on the Chihshang fault. In this study, we aim to answer the following questions: 1) What are the spatial and temporal distributions of repeating earthquakes and what are their relationships to the distribution of seismicity and large earthquakes on the fault? 2) What is the distribution of deep creep rates that can be inferred from Chihshang fault repeating quakes, if they exist? 3) How does deep fault creep inferred from repeating earthquakes compare with deep creep determined geodetically? And 4), how can the repeating earthquake locations, inferred rates, overall seismicity patterns, and distribution of large earthquakes be used to improve our understanding of the earthquake potential in this unique tectonic environment?

2. Data and methodology

2.1. Original catalog

We used 3387 earthquakes from the Central Weather Bureau Seismic Network (CWBSN) catalog. These events occurred in the Chihshang fault region (box, Fig. 1) between 01 January 1991 and the day before the 10 December 2003 M_L 6.4 earthquake. We exclude the 2003 M_L 6.4 aftershocks and subsequent data from this study because the temporal variation in properties of the medium related to large earthquakes may impact the repeating earthquake identification scheme used in this study (time-invariant velocity model). The magnitudes of these catalog events range from M_L 0.78 to 5.42. Magnitude statistics indicate that the CWBSN catalog is complete down to M_L 1.9. Seismograms for these events were recorded by the short-period stations of the CWBSN at sampling rates of 50, 100, and 200 Hz, with rate dependent on the time period of data acquisition. For this study, we used vertical component seismograms from 7 CWBSN stations having relatively low noise level (solid triangles in Fig. 1). Among these stations, only TWF1 and CHK are local to the Chihshang fault, with CHK being closest. A significant fraction of the seismicity occurs offshore. Consequently the station coverage is relatively one-sided. In general, the standard error of the CWBSN epicenters is ~1 km in both horizontal and vertical directions.

2.2. Similar event search

Our first step in searching for repeating events in the Chihshang area involved a comprehensive characterization of event similarity using waveform cross-correlation (Aster and Scott, 1993) and CHK seismograms for all event pairs in the study zone (box, Fig. 1). To reduce the computation effort, only seismograms recorded at CHK station (i.e., the station with the best signal-to-noise ratio for Chihshang fault events) were used.

For most of the study period, CHK seismograms were recorded at 100 samples per second (sps). For the similar events search, those recorded at 50 or 200 sps were re-sampled at 100 sps, and these seismograms were bandpass filtered from 1 to 10 Hz. Maximum cross-correlation coefficient (ccc) between all seismogram pairs were then determined using a 10.5 second window beginning 0.5 s before the P-arrival. Those events having seismogram pairs with ccc's greater than 0.80 were selected as similar event pairs. Similar event pairs were then grouped into similar event clusters whenever pairs shared common events. The resulting event clusters represent an intermediate stage data set from which repeating event sequences were derived.

2.3. Characteristic repeating sequence identification

A basic assumption in deriving deep slip rates from repeating earthquake sequences (Nadeau and McEvilly, 1999) is that events in a given sequence re-rupture the same fault patch and produce earthquakes having similar magnitude, waveforms, and locations. The deep slip method is also most accurate when all repeated ruptures that occurred during the study period have been identified (i.e., the sequences are complete). For deep slip rate estimation in the Chihshang area, it is important to define repeating event sequences that have these properties.

While the similar event clusters derived in the previous section provide a reduced catalog from which repeating sequences can be derived, any given cluster may be comprised of multiple repeating sequences and may also contain additional similar events that do not occur as repeated earthquakes. Further discrimination and decomposition of the similar event clusters into repeating event sequences, therefore, is needed and will be addressed in Section 2.3.2.

2.3.1. Data limitations in the Chihshang area

The relatively sparse and one-sided coverage of the CWBSN stations in the Chihshang area (Fig. 1) coupled with relatively low SNR and unstable noise characteristics (Fig. 2) complicate the task of defining complete and accurate repeating event sequences in this area. During our analysis we have also found that significant origin time errors and/or timing inconsistencies exist in the CWBSN data set, further complicating the task of sequence definition.

Timing errors and timing inconsistencies may have significant impact on earthquake relocation as well as sequence definition in the Chihshang area. The effect can be illustrated by comparing two relocation approaches: (1) double-difference relocation based on standard travel time estimates; (2) double-difference relocation based on travel time estimate using only S–P times and an assumed V_p/V_s

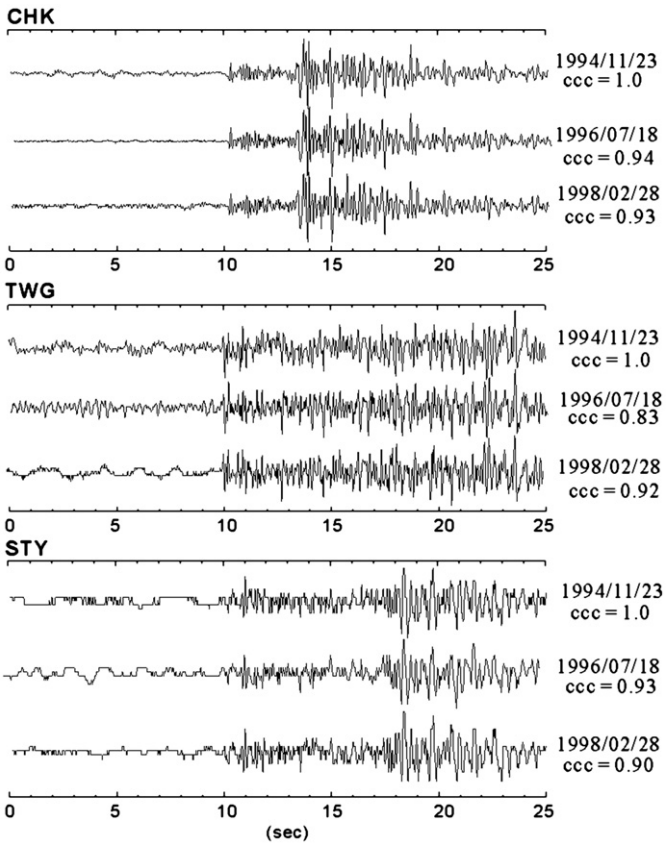

Fig. 2. Typical signal to noise characteristics of the CWBSN stations. Shown are unfiltered vertical velocity seismograms from the 3 events of repeating sequence CH16 (Table 1) recorded at 3 of the 7 stations used in the study. Dates and maximum cross-correlation coefficients (ccc) for 10.5 s data windows starting 0.5 s before P and relative to the reference event (ccc = 1.0) are shown on the right. Signal to noise is good and background noise relatively stable at station CHK (closest to the Chihshang fault). At other stations, however, signal to noise is significantly lower and temporally variable for the events we examined.

velocity model. The later approach, which we refer to as the V_p/V_s method, requires both P- and S-phase alignments, and the assumption of a reasonable V_p/V_s model. Hence it is not always a viable approach for determining relative location of repeating events, especially where the station coverage is sparse and the SNR is marginal. Also, the absolute location accuracy is limited due to the V_p/V_s model assumption. The V_p/V_s method, however, has the distinct advantage of removing the dependency of relocations on catalog origin times and absolute timing inconsistencies among stations in a network. When used in conjunction with similar event data, therefore, the V_p/V_s method can be a useful tool for identifying data plagued with large origin time errors and/or inconsistency in timing among stations.

2.3.1.1. Travel times using S minus P and assumed V_p/V_s. Consider two similar events whose relative P- and S- phase arrival times have been determined using cross-correlation. For standard double-difference relocations (Waldhauser and Ellsworth, 2000), P- and S- travel times (tt_p, tt_s, respectively) are determined by subtracting the origin times of the events from the arrival times. In contrast, the V_p/V_s method determines tt_p, tt_s using the relationships,

$$tt_p = S_mP/((V_p/V_s)-1) \text{ and} \quad (1)$$

$$tt_s = S_mP/(1-(V_s/V_p)) \quad (2)$$

where S_mP is the S minus P time for a given event at a given station and V_p/V_s and V_s/V_p are an assumed V_p/V_s ratio and its reciprocal, respectively. No origin time information is used in determining tt_p and tt_s in these equations, and the dependence on absolute timing accuracy is also reduced to how accurately the rate of sampling between the P and S phase arrivals is maintained. Therefore, assuming accurate sampling over the relatively short interval between S- and P-, Eqs. (1) and (2) can provide travel-time estimates that are largely free of origin time errors and timing inconsistencies among station clocks, both of which can contribute significantly to inaccuracies in relative relocations of earthquakes (Ross et al., 2001); (Rubin, 2002).

It should be pointed out that because an assumed V_p/V_s ratio is used in Eqs. (1) and (2), the absolute locations of relocated events using these equations may not be particularly accurate. However, because we are primarily concerned here with the 'relative' rather than 'absolute' locations of similar events, an assumed V_p/V_s ratio is approximately correct and generally sufficient to assess the degree of location scatter introduced by large origin and inter-station timing errors.

2.3.1.2. Effect of timing errors on relocations in the Chihshang area. The effect of origin and inter-station timing errors on relative locations in the Chihshang area can be illustrated by comparing double-difference relocations (hypoDD (Waldhauser, 2001)) based on standard travel time estimates with those based on travel time estimates from Eqs. (1) and (2) (Fig. 3). In Fig. 3, the same cross-correlation aligned phase data (both P and S, to sub-sample precision) and weighting are used for the hypoDD inversions of a similar event cluster of seven earthquakes using the two types of travel time estimates. A Singular Value Decomposition (SVD) inversion was also used in both cases, and all other inversion parameters are identical. Panels a and b show relocations using travel times calculated by subtracting catalog origin times from cross-correlation aligned phase arrival times (i.e. standard relocations). Panels c through f, show relocations using travel times determined using Eqs. (1) and (2) with an assumed V_p/V_s ratio of 1.78 (i.e., V_p/V_s relocations).

Average horizontal and vertical uncertainties reported by hypoDD for the standard relocations are 290 and 340 m, respectively (Fig. 3a and b). HypoDD uncertainties for the V_p/V_s relocations are generally less than 20 m (Fig. 3c through f). Because all parameters other than the estimated travel-times are identical, the large reduction in location scatter for the V_p/V_s relocations can be attributed primarily to the reduced dependence on origin and/or inter-station timing errors provided by Eqs. (1) and (2).

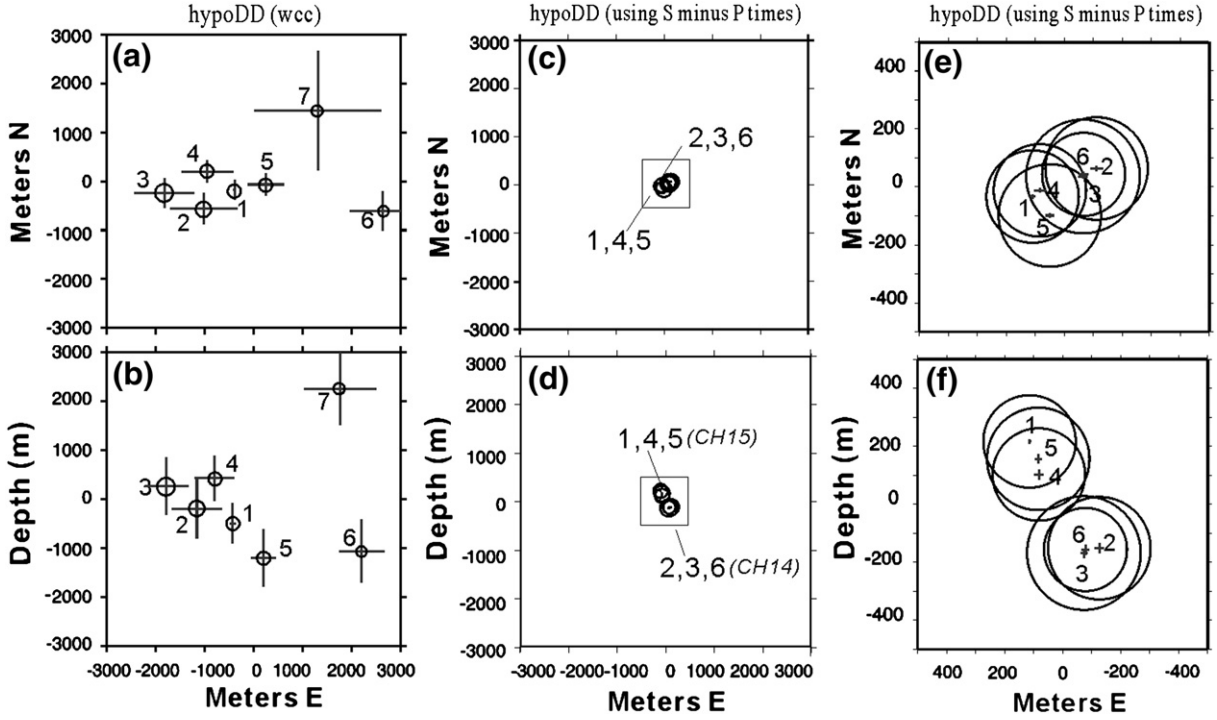

Fig. 3. Double-difference relocations of a similar event cluster (M2.5–2.8) using waveform cross-correlation data (panels a and b), and V_p/V_s method (panels c and d). Panels e and f zoom into locations of interest in panels c and d. Earthquakes are plotted as circles of dimensions corresponding to their magnitude assuming a 3 MPa constant stress drop source. Crosses indicate uncertainties from hypoDD inversion. Note, event seven was excluded as an airquake by the hypoDD inversion (panels c and d). Among the seven stations used in the study, only three stations had high enough waveform similarity to be obtained for event 7. Airquake exclusions are not uncommon when stations coverage is sparse, as in this case.

Table 1
Chihshang repeating sequences

Id	N	Lon (degree)	Lat (degree)	Depth (km)	M_L	T_r (yr)	V_d (cm/yr)
CH1	3	121.384	23.132	16.93	2.2–2.8	1.2–4.3	2.18
CH2	5	121.394	23.144	18.19	1.9–2.9	1.0–2.5	4.28
CH3	3	121.368	23.156	12.61	2.8–2.9	1.8–6.1	2.59
CH4	4	121.393	23.146	17.60	2.8–3	1.0–2.5	3.49
CH5	4	121.395	23.150	18.04	2.9–3.2	1.8–4.1	4.05
CH6	5	121.399	23.153	18.74	2.5–2.8	0.1–3.2	3.99
CH7	3	121.399	23.174	17.60	2.5–3.0	3.0–5.7	2.52
CH8	3	121.401	23.150	18.72	2.5–2.8	2.6–4.5	2.42
CH9	3	121.376	23.153	19.89	3.2–3.6	2.8–5.4	3.65
CH10	3	121.377	23.134	17.00	2.4–2.8	3.2–3.2	2.38
CH11	3	121.377	23.125	16.74	2.7–3.7	1.8–5.0	3.41
CH12	3	121.374	23.208	12.74	2.1–2.3	2.7–4.4	1.85
CH13	3	121.435	23.150	22.55	2.1–2.9	0.8–2.6	2.34
CH14	3	121.426	23.161	21.19	2.5–2.8	2.5–3.3	2.39
CH15	3	121.404	23.162	19.70	2.6–2.7	1.3–4.1	2.35
CH16	3	121.389	23.230	13.48	2.1–2.2	1.6–1.7	1.83
CH17	3	121.336	23.164	7.09	2.1–2.3	1.8–2.9	2.37
CH18	4	121.413	23.153	10.88	2.1–3.0	1.0–4.0	3.27
CH19	3	121.384	23.197	13.89	2.0–2.3	1.4–3.8	1.84
CH20	5	121.438	23.157	21.67	2.5–2.6	1.2–2.4	3.71
CH21	7	121.376	23.133	16.2	2.0–2.4	0–4.0	4.22
CH22	3	121.410	23.214	20.59	2.1–2.3	0.4–1.4	1.85
CH23	3	121.336	23.164	7.09	2.1–2.3	1.8–2.9	1.85
CH24	4	121.402	23.179	17.865	2.0–3.0	1.2–3.9	3.03
CH25	3	121.404	23.156	19.41	2.3–2.5	2.0–3.1	2.10
CH26	3	121.396	23.163	18.215	2.5–3.0	2.6–3.0	2.43
CH27	4	121.404	23.163	19.70	2.6–2.7	0.4–2.5	3.09
CH28	4	121.364	23.151	12.85	2.3–2.5	1.6–3.1	2.71
CH29	4	121.335	23.105	11.96	2.5–2.8	2.2–3.1	3.06
CH30	5	121.373	23.160	15.34	2.1–3.0	1.2–3.4	3.95

N: number of repeating events in a given repeating sequence.
Lon, Lat, and Depth: average location in each repeating sequence.
M_L: local magnitude unit.
T_r: Range of recurrence times for the sequence.
V_d: Long-term slip rate (described in the text of Section 5).

The V_p/V_s relocations also show that what had originally appeared to be seven earthquakes with distinctly different locations in the standard relocation results actually resolve themselves into two sites with three events each that are primarily overlapping. The remaining event was excluded by hypoDD as an airquake (i.e., an earthquake that locates above the ground after relocation, which is due to the original near-surface location and the lack of control in vertical offset between the events (Waldhauser, 2001)). We eventually identified the overlapping events at the two sites as members of two different repeating sequences (CH14 and CH15 in Table 1), and determined that the airquake did not belong to an identifiable repeating sequence.

Additional tests using other similar event clusters indicate that the exclusion of events by hypoDD and the timing and associated relative location errors illustrated by the example in Fig. 3 are fairly common for the Chihshang area. These errors in conjunction with the sparse and one-sided coverage of the CWBSN stations, intermittent station outages for the sparse network, and the temporally unstable noise characteristics of the CWBSN records (Fig. 2) make comprehensive and systematic identification of Chihshang repeating events using a location based approach impractical.

The accuracy of repeating event identification based solely on a waveform similarity criteria is also somewhat limited for small magnitude repeaters in the Chihshang area due to the small number of stations, the large variation in event-to-station travel paths, and the generally low and temporally variable SNR.

2.3.2. Composite selection criteria

Given the limited quantity and quality of seismic data and the need to identify repeating event sequences as accurately and completely as possible for inferring deep fault slip rates, we have chosen a more robust approach for identifying repeating event sequences in the Chihshang area, called 'composite selection approach'. The approach incorporates both waveform similarity (as measured using 'ccc' between repeating events) and differential S-P (dS_mP) time information at sub-sample precision, which allows exclusion of outliers in the ccc and dS_mP data. By relying only on ccc and dS_mP time statistics on a station by station basis, the method also effectively eliminates errors introduced by inaccurate origin times and inter-station timing.

Two key observables of earthquakes re-rupturing the same fault patch are their effective co-location and the similarity of their seismograms throughout the P-, S- and coda phases. The composite selection approach constrains repeated event locations by requiring the dS_mP times between repeating event pairs to be small, and

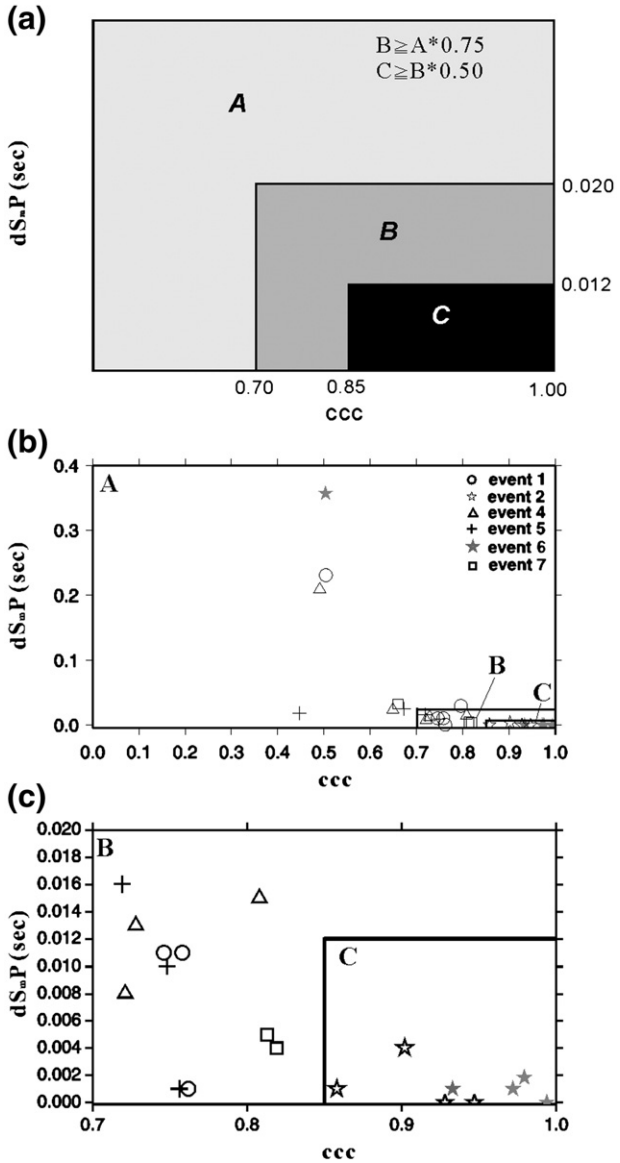

Fig. 4. (a) Schematic illustration of the criteria used for repeating earthquake identification in the study area. 'dS_mP' is the difference in S–P time between two events. 'ccc' is the maximum cross-correlation coefficient between two events. Region A is the area for all measurements, region B is the area of ccc≧0.70 and dS_mP≦0.02, and region C is the area of ccc≧0.85 and dS_mP≦0.012. (b) Ccc, dS_mP statistics for a group of similar events (location shown in Fig. 3) compared to event 3. Each point maps the dS_mP and ccc for an event pair at a single station. Points with identified symbols are for the same event paired with event 3. (c) Zoom in of region B. Event 2 and 6 pass the selected criteria discussed in the text, and therefore are grouped into a repeating sequence with event 3. Those three repeating events belong to sequence CH14 in Table 1.

constrains seismogram similarity by requiring the ccc to be high for a long data window and over a broad frequency band.

In an idealized situation, where repeating event ruptures are identical, noise contributions are non-existent, and propagation and recording characteristics are time invariant, dS_mP times between repeated events should be zero and their seismograms should be identical (e.g., ccc≅1) at all stations. In nature, however, subtle yet significant temporal variations in propagation velocities are known to occur (Rubin, 2002) as are small variations between the ruptures of repeating events (e.g., seismic moments (Vidale et al., 1994; Nadeau and Johnson, 1998; Nadeau and McEvilly, 1999). Such variations translate into deviations from idealized expectation in the dS_mP time and ccc measurements for repeating events. These deviations are generally relatively minor when data quality is good, and there is usually a clear distinction in dS_mP time and ccc statistics between the repeating and non-repeating event-pairs. This distinction can be used as a basis for repeating event identification.

When the data quality is lower (e.g., in the Chihshang area), the distinction between repeated and non-repeated event statistics is less clear and unless compensated for can confound efforts to accurately define repeating event sequences. To compensate for the lower data quality in the Chihshang area, therefore, we take the approach of reducing the sensitivity of our identification scheme by excluding statistical outliers.

This is done in the following manner: First, we define an event similarity space [dS_mP, ccc] (Fig. 4). We then populate this space with similarity point measurements (dS_mP, ccc) where each point represents the dS_mP and ccc measurements between two events for a given station. All event pair combinations for a similar event group are considered. Ccc statistics are determined using a 10.5 second window beginning 0.5 s before the P-arrival using a bandpass filter of 2–18 Hz. 'dS_mP' statistics were determined using two 2.5 second windows beginning 0.5 s before the P-arrival and the S-arrival.

Due to the true differences between event sources and noise inherent in the data, deviations of the similarity points from idealized expectations generally occur. We therefore break the similarity space into three regions as shown in Fig. 4a. Region A is the area for all measurements, region B is the area of ccc≧0.70 and dS_mP≦0.02, and region C is the area of ccc≧0.85 and dS_mP≦0.012. Region C represents (dS_mP, ccc) data with the highest degree of similarity.

Fig. 4b and c show the ccc and dS_mP statistics for a group of similar events compared to event 3. Their V_p/V_s relocations are shown in Fig. 3. The (dS_mP, ccc) points clustered in region C correspond to the co-located events 2, 3, and 6 from relocation result in Fig. 3. Whereas the (dS_mP, ccc) points outside region C correspond to the events 1, 4, and 5, which are ~200 m away from events 2, 3, and 6. One may question the necessity of using dS_mP as a criterion since high enough ccc seem to correspond with small dS_mP as shown in Fig. 4c. Nevertheless a small fraction of similarity points for true repeating events may plot outside region C in some situations, e.g., poor quality of station data or small P (or S) amplitude. In such cases both criteria in dS_mP and ccc are necessary. In Supplementary Figs. S1 and S2 we show the relocation and ccc, dS_mP statistics from another similar event cluster, which demonstrating that misidentification may occur if the analysis solely replies on the ccc criterion.

To help compensate for the ambiguity in identifying repeated events, we carry out a series of empirical tests that defines the fraction of similarity points (dS_mP, ccc) in region C and region B using earthquake co-location as a constraint. The criteria are selected when we reach a consistent result using overall similar event clusters. Consequently we use the following composite criteria for defining repeated event pairs within a similar event group: For two events to be considered a repeating pair at least 75% of their similarity points must lie within region B, and of those points at least 50% must also lie within region C. Once repeating pairs have been selected, they are organized into repeating event sequences. Each sequence is a collection of events that are linked by the composite criteria to at least one other member of the sequence.

3. Repeating earthquake distributions

Using the composite selection criteria described above, we identified 30 repeating sequences in the Chihshang area containing 109 repeating events with magnitudes ranging from 1.9 to 3.7 (Table 1). Each sequence has three to seven repeating events (event chronologies are shown in Supplementary Fig. S3). The sequences composed of only two events are excluded from our repeating event data set. The observed repeating events represent about 3% of all the M 1.9 to 5.4 earthquakes in the starting catalog. Fig. 5 shows examples of the waveforms for one repeating sequence. Locations of the 30 repeating sequences are shown in Fig. 1 and Fig. 6. All the repeating sequences occur within the depth range 7 to 23 km, and tend to concentrate on the northern portion of the Chihshang segment (north of 23.1°N).

The Chihshang area experienced two M>5 events during the study period. In 1992 a M_L 5.4 event occurred at relatively shallow depth on the northern segment and in 1995 a deeper M_L 5.3 event occurred on the southern segment. Shortly after the end of the study period a M_L 6.4 event occurred (10 December 2003) and was located between the two M>5 earthquakes. The hypocenters of the repeating sequences tend to occur away from the aftershock zones of the M>5 events (Fig. 6).

The distribution of recurrence intervals and their coefficients of variation (standard deviation divided by the mean) for the 30 repeating sequences are shown in Fig. 7. The coefficient of variation (COV) results indicate that for the most part, events in the Chihshang area occur quasi-periodically (COV of 0 implies perfect periodicity,

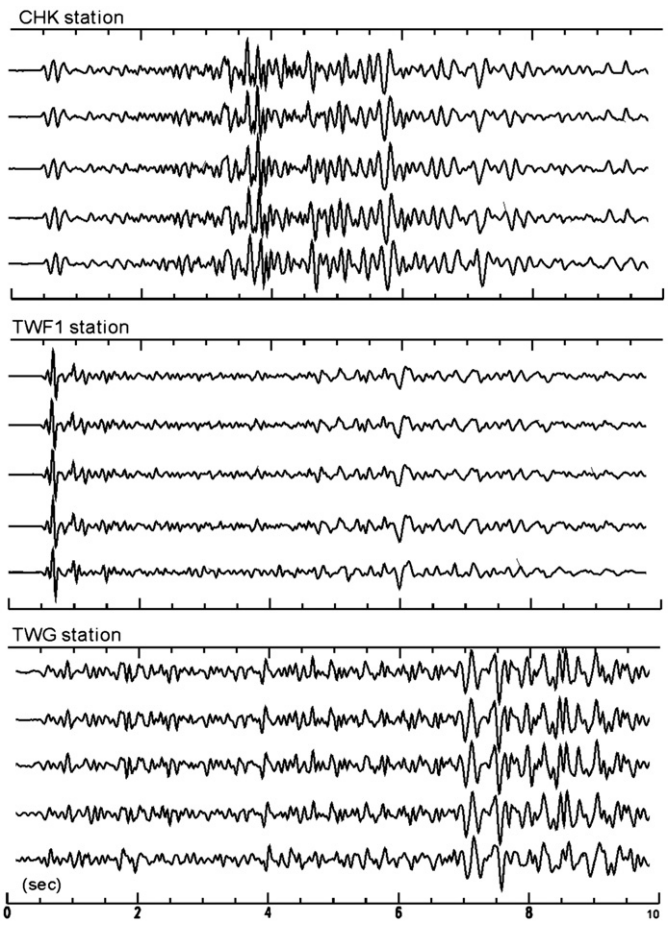

Fig. 5. Filtered 2–18 Hz waveforms recorded at station CHK, TWF1, and TWG from repeating sequence CH2. Each trace is normalized by its maximum amplitude.

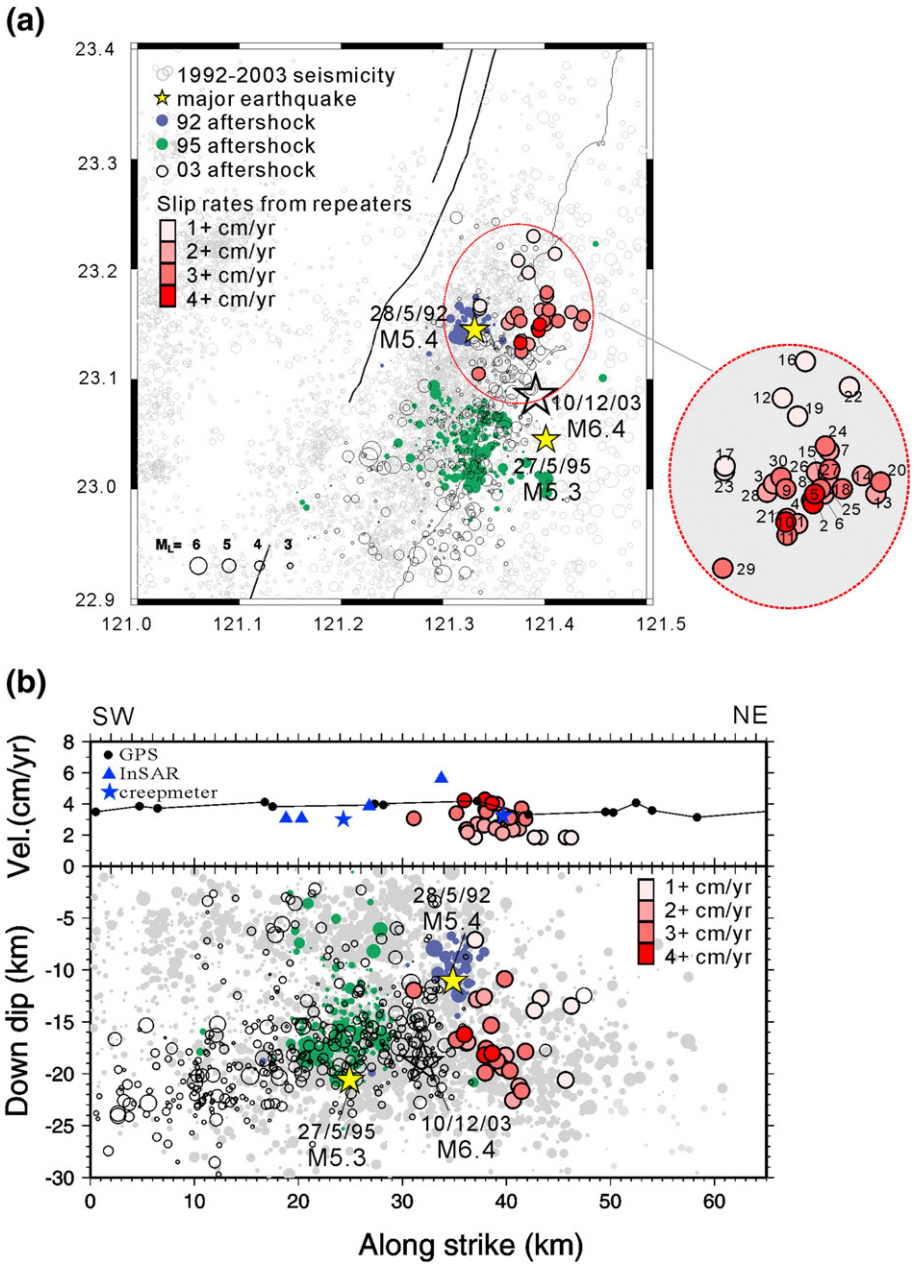

Fig. 6. (a) The spatial distribution of repeating sequence derived slip rates in mapview. Filled circles with a black rim represent locations of repeating sequences. Fill colors/shades are keyed to the slip rates. Yellow stars indicate major events during the study time period from 1992–2003 December. Open star indicates the event that occurred on 10 December 2003 just after the study period. Background seismicity is indicated by gray circles. Aftershock sequences from the 1992 and 1995 *M* 5+ events are shown as blue and green circles without a rim, respectively. (b) Lower panel: the spatial distribution of repeating sequence derived slip rates in along-strike cross-section. Upper panel: filled squares with a black rim show a projection of repeaters on the along-strike distance and their corresponding slip rates. Black dots shows combined surface slip rates from GPS and leveling data measurement. Line connecting each GPS data indicates the average value. Blue solid triangles and stars are along-dip projection of InSAR data (Hsu and Bürgmann, 2006) and creepmeter data (Lee et al., 2003).

COV≅1 implies Poissonian recurrence and COV>1 indicates temporal clustering).

A clear majority of the recurrence intervals are also longer than ~1 year (consistent with a renewal process for deformation rates and repeating event magnitudes on the Chihshang fault). However, several intervals are as short as 0.1 years or less. Because the Chihshang repeating sequences occur away from the two $M>5$ events and because the terminal events of the short intervals are not correlated in time with the $M>5$ events nor their aftershocks, it does not appear that the short intervals result from accelerated post-seismic creep related to the larger events. Therefore, these <0.1 yr recurrence intervals are excluded from the creep rate estimates in the following section.

Short recurrence intervals of similar duration have been observed for similar and repeating event sequences on the San Andreas and Hayward faults at Parkfield and in the Bay Area of California (Nadeau et al., 1995; Waldhauser and Ellsworth, 2002; Templeton et al., 2007). They have been interpreted to be the result of a triggering or micro-aftershock process occurring between events on closely spaced but non-overlapping fault patches. Since triggering is a non-renewing process, the short intervals suggest that a few of our repeating sequences may be contaminated with events that are not occurring on the same fault patch. This is not surprising given the relatively low data quality and small magnitudes of the sequence events.

4. Spatio-temporal creep rate variations

Deep fault creep rates can be inferred using the recurrence intervals and seismic moments of repeating sequence events (Nadeau

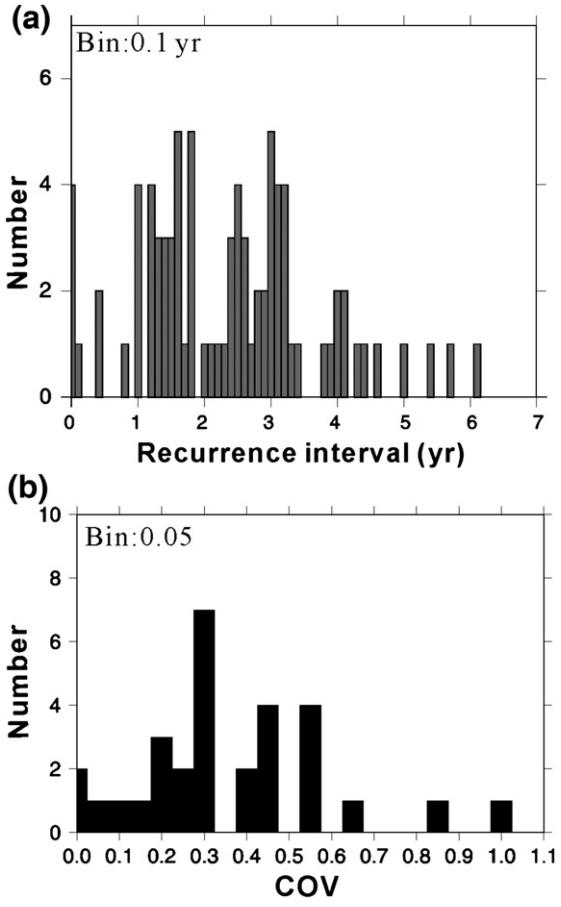

Fig. 7. (a) Histogram of recurrence intervals for the 109 repeating events. (b) Histograms of coefficient of variation in recurrence intervals for the 30 sequences.

and Johnson, 1998; Nadeau and McEvilly, 1999; Matsuzawa et al., 2002; Uchida et al., 2003; Nadeau and McEvilly, 2004). The method first relates the seismic moment of a repeated event (M_0) to the surrounding aseismic fault slip (d_i) that loads the event's rupture patch to failure during its preceding recurrence interval. In other words, d_i represents the creep on the surrounding fault area that has taken place since the last event on the repeating patch.

$$d_i = 10^{\alpha} M_0^{\beta} \tag{3}$$

This relationship is then used in conjunction with the preceding recurrence intervals (T_r) or observation period (T_{obs}) to infer short- or long-term fault creep rates ($V_d(i)$ and V_d, respectively).

$$\text{Short–term: } V_d(i) = \sum_{i=2}^{N} d_i / \sum_{j=1}^{N-1} T_r(i) \tag{4}$$

$$\text{Long–term: } V_d = \sum_{i=1}^{N} d_i / T_{obs} \tag{5}$$

where N is the number of events in the sequence, i and j refers to individual events and recurrence intervals in a sequence, respectively. In conjunction with the locations of the repeating sequences the rates can then be used to map out the spatial and temporal distribution of fault creep rates at depth. For estimating deep fault creep rates in the Chihshang area, α=−2.36±0.16 and β=0.17±0.01 in Eq. (3). These parameters were empirically derived from earthquake and geodetic data at Parkfield, California (Nadeau and Johnson, 1998), and have also been used to infer deep slip rates in other regions outside Parkfield (e.g., along the Japan subduction zone (Matsuzawa et al., 2002; Uchida et al., 2003; Igarashi et al., 2003)). Seismic moments for the Chihshang area data were derived from the CWBSN earthquake magnitude catalog (M_L) using the following empirical equations,

$$M_w = (0.9 \pm 0.03) M_L + (-0.07 \pm 0.15) \text{ (Huang et al., 2000)} \tag{6}$$

$$M_w = (\log M_0 / 1.5) - 10.73 \text{ (Hank and Kanamori, 1979)} \tag{7}$$

where M_w is moment magnitude and M_L is local magnitude.

In Fig. 8a, the depth distribution of the short-term and long-term creep rates indicates that the two measurements have a similar range of values (2–5 cm/yr) except for few points that show >6 cm/yr short-term rates. The short-term rates appear to vary with depth, whereas the long-term rates likely remain in a small range of 2–4 cm/yr. The largest difference between the two rates appears at 20 km depth, where we found the anomalously high short-term rate (~8 cm/yr) is from the short-lived sequence CH22 (i.e., lifetime=1.8 yr, from February 1997 to December 1998). To examine whether the depth-dependent trend is due to a biased measurement from the sequences characterized by the relatively short lifetime, we show how the short-term rate varies with repeater's lifetime in Fig. 8b. The result indicates that the very short lifetime contributes to the larger short-term estimates. This suggests that one should expect the long-term and short-term creep rates to be the same if the repeating events span the entire observation period. The temporally clustered sequences are less complete in time and generally lead to large uncertainty in the creep rate estimates. Because long-term creep rate estimates are less scattered and more stable than short-term rates, we use the long-term estimate to illustrate the spatial distribution of creep rate at each repeating sequence site.

The locations, number of events, magnitudes, seismic moments, and recurrence intervals of the 30 repeating sequences are listed in Table 1, and the resulting deep creep rates are shown by filled circles in Fig. 6. The creep rate estimates range from 1.8–4.3 cm/yr with an average of 3 cm/yr. The highest creep rates (above 4 cm/yr) are found

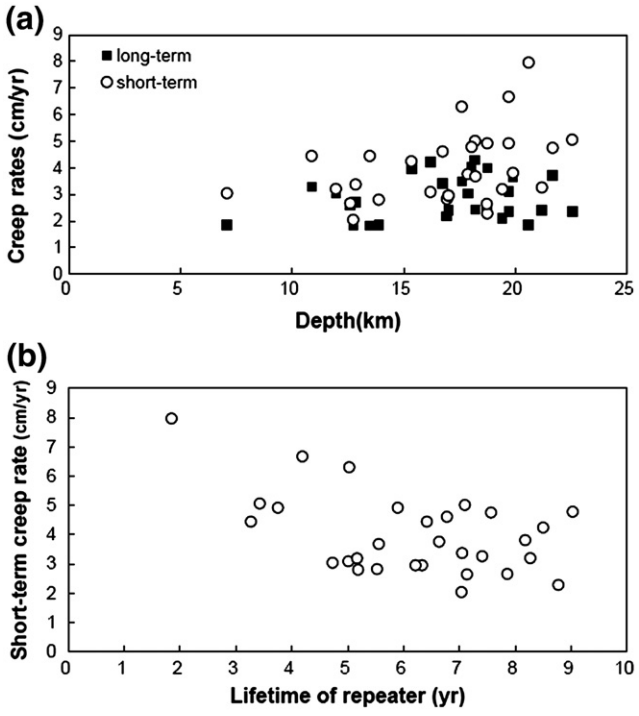

Fig. 8. (a) Creep rate estimates as a function of depth. Filled squares and open circles indicate the long-term and short-term rates separately. (b) Short-term creep rate versus repeater's lifetime.

on the deep portion of the fault, between 16 and 18 km, and creep rates of less than 2 cm/yr are distributed from 7–21 km depth. The overall creep rates estimates do not reveal a systematic depth-dependent behavior. In the upper panel of Fig. 6b, we compare the along-strike variation of deep creep rates with surface observations. Black dots labeled 'GPS' are actually the slip rates estimated from a combination of the average uplift rate from 1985–1994 leveling data (Liu and Yu, 1990; Yu et al., 1990) and horizontal deformation rate from 1992–1999 GPS data (Yu and Kuo, 2001). The InSAR data (Hsu and Bürgmann, 2006) and creepmeter data (Lee et al., 2003) are projected into the along-dip direction assuming a fault dip angle of 60° for the shallow portion of the fault (Kuochen et al., 2004). The above surface measurements (particularly creep) are consistent with the deep repeating earthquake creep rates (~3 cm/yr). This correlation supports the validity of applying Eq. (3) to the Chihshang fault and suggests that the empirical relationship derived from Parkfield's repeating earthquakes data is also applicable to regions other than the San Andreas fault.

The times and slips for different repeating sequence sites (Fig. 9a) are used to infer temporal variation in slip rates. We first compute the cumulative slip of all sequences through time, then the cumulative slips were divided by the number of repeating sequences (Fig. 9 b) (Nadeau and McEvilly, 2004). To obtain the slip rates, the normalized cumulative slips are next divided by 1-year time intervals with a 1-year running window stepped in 0.5-year intervals. In Fig. 9c (top panel), the result indicates the computed slip rates first increased to 5 cm/yr in mid-1994 and suddenly dropped to 2 cm/yr, then returned to 4–5 cm/yr during 1996–1998. Soon after 1998, slip rates gradually decreased to 3 cm/yr then maintained 2–3 cm/yr afterward. The temporal pattern of creep rates are compared with background seismicity rates for the entire study area (bottom panel in Fig. 9c) and the repeating sequences area (center panel in Fig. 9c). On May 1995, owing to the 1995 M 5.3 mainshock in the southern portion of the fault, consistent peaks in seismicity rates are observed at both of the study area and the repeaters area. A decrease of deep creep rate, however, occurred at the same period, which inversely correlates to earthquake activity in mid-1995. The timing of deep creep rate pulses after 1996 shows better visual correlation with the seismicity rates of the repeaters area. This suggests that the relation between accelerated quasi-static slips of small repeating events and the 1995 M 5 event is not apparent. However, the temporal variation of slip rates is likely associated with nearby background seismicity. What controls the time histories of deep slip rate and as well as background seismicity is not yet clear and requires further analysis.

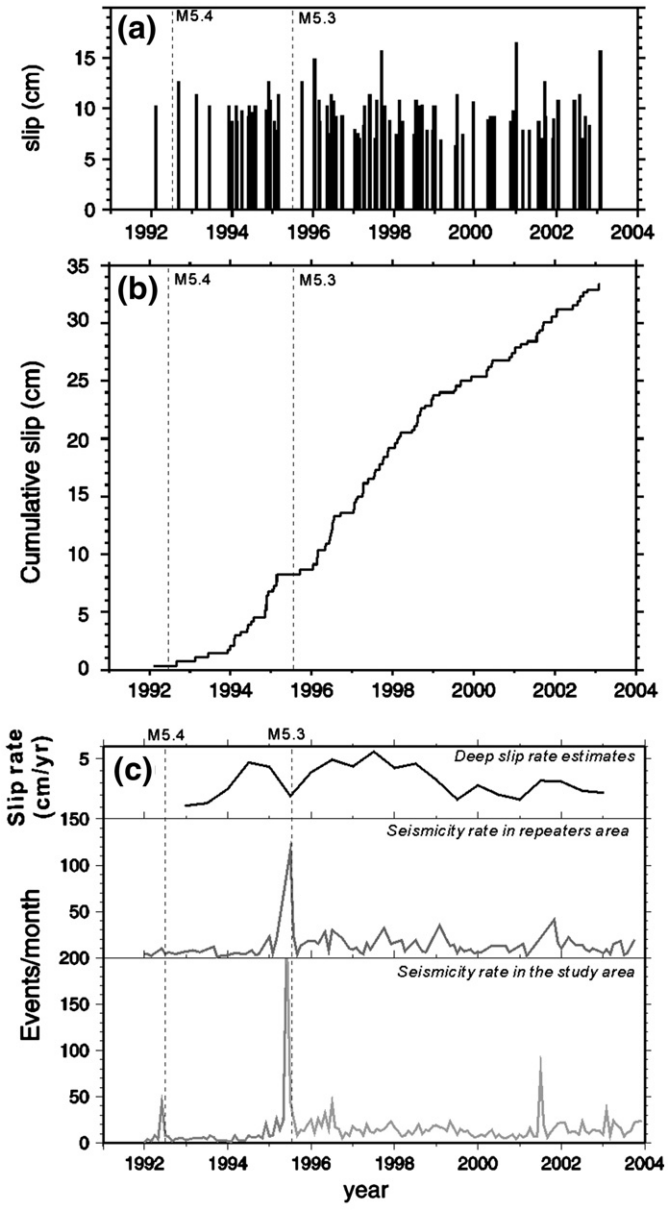

Fig. 9. (a) Compilation of slip estimates from 113 repeating earthquakes and their corresponding time. (b) Normalized cumulative slip as a function of time. (c) Top panel: temporal distribution of deep slip rates from repeating sequences smoothed with a 1-yr running window overlapped by 0.5-year. Center panel: seismicity rate as a function of time in the area showing repeating events (23.10°N–23.23°N, 121.33°E–121.44°E, 7–23 km at depth). Bottom panel: seismicity rate as a function of time in the entire study area (see the box in Fig. 1). Dashed lines indicate two $M>5$ events.

5. Fault behavior

It is generally accepted that repeating events are located on the edge of or away from larger asperities and are caused by repetitive rupture of small asperities surrounded by stable sliding areas (Beeler et al., 2001; Sammis and Rice, 2001; Johnson and Nadeau, 2002; Nadeau and McEvilly, 2004). Regions of seismically active but non-repeating events could be either creeping or locked. In Parkfield, the transition from locked to creeping behavior is shown by along-strike variation of surface slip rates, which can be well correlated with the slip rates derived from repeating earthquakes (Nadeau and McEvilly, 1999).

The northern section of the Chihshang fault (north of 23.1°N) where the 30 repeating sequences took place, is likely a weakly coupled (i.e., low level of friction) area because the 3 cm/yr averaged slip rate at depth is comparable to the surface rate. Since continuous loading through stable-sliding material is the key mechanism for repeated rupture on the same spots, we interpret the northern area encompassing the repeating sequence and background seismicity as stable-sliding area. It is worth noting that the subsequent 2003 M_L 6.4 mainshock occurred at the southern edge where the repeaters stop, and its aftershock (open circles in Fig. 6) generally extended southward from the hypocenter to avoid the repeating section. Geodetically derived co-seismic slip is modeled to be dominant in southern portion of the fault (Hu et al., 2007), which implies that fault creep may be restricted at the northern segment. The southern section which has no repeating earthquakes, and is the location of the major slip from the M_L 6.4 event, is inferred as a strongly coupled area (i.e., locked, which generate large amplitudes of slip co-seismically).

According to creep meter data from 1998 to 2003, the coupling of the fault slip is relatively strong in the dry season. The fault creeps steadily during the rainy season and remains locked in the dry season, while microearthquake activity is active at a depth range of 10–25 km without seasonal variation (Lee et al., 2001; Lee et al., 2003). The difference in the temporal occurrence of surface creep and subsurface seismicity indicates the strong fault coupling at the near surface. The

stress that accumulated at greater depth was partially released during the wet season and stored during the dry season, which may have eventually reached a critical condition that produced the 2003 M_L 6.4 Chengkung earthquake on this fault segment.

6. Conclusion

We have found repeating earthquakes on an imbricated reverse fault in the arc-continent collision boundary of eastern Taiwan, the Chihshang fault. The Chihshang fault creeps at the surface with a high rate of 2–3 cm/yr and slips in large earthquakes. To improve seismic hazard assessment, it is important to know how the creep rate observed at the surface is related to the fault slip rate at depth. The recently discovered repeating earthquakes in the Chihshang area offer a new insight into deep fault behavior. We have shown that the repeating events are located in the northern half of the fault, indicating the fault property in this portion is probably different from that in the south. The 30 repeating sequences occurred at 7–23 km depth with 3 cm/yr average deep slip rate consistent with surface creep rate, suggesting that the creeping section probably extends from near surface to the depth of 23 km in the north. We infer a contrasting deep fault slip behavior from north to south on the Chihshang fault. The northern segment is creeping and the southern segment is partially locked with a higher earthquake potential, consistent with the occurrence of the 2003 M 6 event.

In this study, we also pay particular attention to developing a proper identification scheme because the high noise level of the seismic data and low station coverage in this area could have significant impact on the identification of repeating earthquakes. We propose an objective composite selection criterion to identify repeating sequences. Considering the criteria in both S-P differential time and waveform similarity, this method provides an independent check on repeating events decomposition. The repeating sequence identification using composite selection criteria has an obvious advantage when poor station coverage and low signal to noise level are present.

Acknowledgements

We thank Honn Kao for motivating the study, Wen-Tzong Liang for the guidance on programming, and Jyr-Ching Hu for his internal reviews. We are grateful to Jian-Cheng Lee, Toru Matsuzawa, Naoki Uchida, Bill Ellsworth, Hiroo Kanamori, Shinji Toda, Charles Lewis, Roland Bürgmann, Leslie Hsu, Yih-Min Wu, and Nicolas Houlie for their helpful discussions. We also thank two reviewers for their helpful comments. This research was partially supported by Taiwan NSC grant 96-2116-M-006-011.

Appendix A. Supplementary data

Supplementary data associated with this article can be found, in the online version, at doi:10.1016/j.epsl.2008.09.021.

References

Angelier, J., Chu, H.T., Lee, J.C., 1997. Shear concentration in a collision zone: kinematics of the active Chihshang fault, Longitudinal Valley Fault, eastern Taiwan. Tectonophysics 247, 117–144.
Angelier, J., Chu, H.T., Lee, J.C., Hu, J.C., 2000. Active faulting and earthquake hazard: the case study of the Chihshang Fault, Taiwan. J. Geodyn. 29, 151–185.
Aster, R.C., Scott, J., 1993. Comprehensive characterization of waveform similarity in microearthquake data sets. Bull. Seismol. Soc. Am. 83, 1307–1314.
Barrier, E., Chu, H.T., 1984. Field Trip Guide to the Longitudinal Valley and the Coastal Range in Eastern Taiwan, in Sino-French colloquium, pp. 27–49.
Beeler, N.M., Lockner, D.L., Hickman, S.H., 2001. A simple stick-slip model for repeating earthquakes and its implication for microearthquakes at Parkfield. Bull. Seismol. Soc. Am. 91, 1797–1804.
Beroza, G.C., Cole, A.T., Ellsworth, W.L., 1995. Stability of coda wave attenuation during the Loma Prieta, California, earthquake sequence. J. Geophys. Res. 100, 3977–3988.
Bürgmann, R., Schmidt, D., Nadeau, R.M., d'Alessio, M., Fielding, E., Manaker, D., McEvilly, T.V., Murray, M.H., 2000. Earthquake potential along the Northern Hayward Fault, California, Science 289, 1178–1182.
Cheng, S.N., Yeh, Y.T., Yu, M.D., 1996. The 1951 Taitung earthquake in Taiwan. J. Geol. Soc. China 39, 267–285.
Chen, H.H., Rau, R.J., 2002. Earthquake locations and focal mechanisms in an active arc-continent plate boundary: the Chihshang Fault of eastern Taiwan. EOS Trans. AGU Fall Meet. Suppl. 83 (47), F1281.
Chu, H.T., Lee, J.C., Angelier, J., 1994. Non-seismic rupture of the Tapo and the Chinyuan area on the southern segment of the Huatung Longitudinal Valley Fault. eastern Taiwan in Annual meeting of Geol. Soc. China, Taipei, pp. 1–5.
Ellsworth, W.L., Dietz, L.D., 1990. Repeating earthquakes: characteristics and implications, Proc. of Workshop. XLVI, the 7th U.S.–Japan Seminar on Earthquake Pred., U.S. Geol. Surv. Open-File Rept. 90–98, 226–245.
Hank, T.C., Kanamori, H., 1979. A moment magnitude scale. J. Geophys. Res. 84, 2348–2350.
Hsu, L., Bürgmann, R., 2006. Surface creep along the longitudinal Valley fault, Taiwan from InSAR measurements. Geophys. Res. Lett. 33. doi:10.1029/2005GL024624.
Hsu, T.L., 1962. Recent faulting in the Longitudinal Valley of eastern Taiwan. Memoir Geol. Soc. China 1, 95–102.
Huang, K.C., Kao, H., Wu, Y.M., 2000. The determination of M_L–M_W in Taiwan, 8th Annual Meeting of Geophysical Society of China, pp. 193–201. in Chinese.
Hu, J.C., Cheng, L.W., Chen, H.Y., Wu, Y.M., Lee, J.C., Chen, Y.G., Lin, K.C., Rau, R.J., Kuochen, H., Chen, H.H., Yu, S.B., Angelier, J., 2007. Coseismic deformation revealed by inversion of strong motion and GPS data: the 2003 Chengkung earthquake in eastern Taiwan. Geophys. J. Int. 169, 667–674.
Igarashi, T., Matsuzawa, T., Hasegawa, A., 2003. Repeating earthquakes and interplate aseismic slip in the northern Japan subduction zone. J. Geophys. Res. 180. doi:10.1029/2002JB001920.
Johnson, P.A., Nadeau, R.M., 2002. Asperity model of an earthquake: static problem. Bull. Seismol. Soc. Am. 92, 672–686.
Kuochen, H., Wu, Y.M., Chang, C.H., Hu, J.C., Chen, W.S., 2004. Relocation of eastern Taiwan earthquakes and tectonic implications. Terr. Atmos. Ocean. Sci. 15, 647–666.
Lee, J.C., Structure of deformation active d'un orogene: Taiwan, Mem. Sc. Terre thesis, Université Pierre et Marie Curie (1994).
Lee, J.C., Angelier, J., Chu, H.T., Hu, J.C., Jeng, F.S., 2001. Continuous monitoring of an active in a plate suture zone: a creepmeter study of the Chihshang Fault, eastern Taiwan. Tectonophysics 333, 219–240.
Lee, J.C., Angelier, J., Chu, H.T., Hu, J.C., Jeng, F.S., Rau, R.J., 2003. Active fault creep variations at Chihshang, Taiwan, revealed by creep meter monitoring, 1998–2001. J. Geophys. Res. 108. doi:10.1029/2003JB002394.
Lee, J.C., Chu, H.T., Angelier, J., Hu, J.C., Chen, H.Y., Yu, S.B., 2006. Quantitative analysis of surface coseismic faulting and postseismic creep accompanying the 2003, M_w = 6.5, Chengkung earthquake in eastern Taiwan. J. Geophys. Res. 111. doi:10.1029/2005JB003612.
Liu, C.C., Yu, S.B., 1990. Vertical crustal deformations in eastern Taiwan and its tectonic implications. Tectonophysics 183, 111–119.
Massonnet, D., Rossi, M., Carmona, C., Adragna, F., Peltzer, G., Feigl, K., Rabaute, T., 1993. The displacement field of the Landers earthquake mapped by radar interferometry. Nature 364, 138–142.
Matsubara, M., Yagi, Y., Obara, K., 2005. Plate boundary slip associated with the 2003 Off-Tokachi earthquake based on small repeating earthquake data. Geophys. Res. Lett. 32. doi:10.1029/2004GL022310.
Matsuzawa, T., Igarashi, T., Hasegawa, A., 2002. Characteristic small-earthquake sequence off Sanriku, northern Honshu, Japan. Geophys. Res. Lett. 29. doi:10.1029/2001GL014632.
Nadeau, R.M., Johnson, L.R., 1998. Seismological studies at Parkfield VI: moment release rates and estimates of source parameters for small repeating earthquake. Bull. Seismol. Soc. Am. 88, 790–814.
Nadeau, R.M., McEvilly, T.V., 1999. Fault slip rates at depth from recurrence intervals of repeating microearthquakes. Science 285, 718–721.
Nadeau, R.M., McEvilly, T.V., 2004. Periodic pulsing of characteristic micro-earthquakes on the San Andreas fault. Science 303, 220–222.
Nadeau, R.M., Foxall, W., McEvilly, T.V., 1995. Clustering and periodic recurrence of microearthquakes on the San Andreas fault at Parkfield, California. Science 267, 503–507.
Poupinet, G., Ellsworth, W.L., Fréchet, J., 1984. Monitoring velocity variations in the crust using earthquake doublets: an application to the Calaveras fault, California. J. Geophys. Res. 89, 1179–1189.
Ross, S.L., Michael, A.J., Ellsworth, W.L., Julian, B., Klein, F., Oppenheimer, D., Richards-Dinger, K., 2001. Effects of initial location error and station distribution on double-difference earthquake relocation: comparing the San Gregorio and Calaveras faults. Seism. Res. Lett. 72, 291–292.
Rubin, A.M., 2002. Using repeating earthquakes to correct high-precision earthquake catalogs for time-dependent station delays. Bull. Seismol. Soc. Am. 92, 1647–1659.
Sammis, C.G., Rice, J.R., 2001. Repeating earthquakes as low-stress-drop events at a border between locked and creeping fault patches. Bull. Seismol. Soc. Am. 91, 532–537.
Savage, J.C., Lisowski, M., 1993. Inferred depth of creep on the Hayward fault, central California. J. Geophys. Res. 98, 787–793.
Simpson, R.W., 2000. Watching the Hayward Fault. Science 289, 1147–1148.
Templeton, D.R., Nadeau, M., Bürgmann, R., 2007. Behavior of repeating earthquake sequences in central California and the implications for subsurface fault creep. Bull. Seismol. Soc. Am. 98, 52–65.
Uchida, N., Matsuzawa, T., Hasegawa, A., 2003. Interplate quasi-static slip off Sanriku, NE Japan, estimated from repeating earthquakes. Geophys. Res. Lett. 30. doi:10.1029/2003GL017452.

Vidale, J.E., Ellsworth, W.L., Cole, A., Marone, C., 1994. Variations in rupture process with recurrence interval in a repeated small earthquake. Nature 368, 624–626.
Vidale, J.E., Ellsworth, W.L., Cole, A., Marone, C., 1994. Variations in rupture process with recurrence interval in repeated small earthquakes. Nature 368, 624–626.
Waldhauser, F., 2001. hypoDD — a program to compute double-difference hypocenter locations. U.S. Geol. Surv. Open-File Rep. pp. 1–113.
Waldhauser, F., Ellsworth, W.L., 2000. A double-difference earthquake location algorithm: method and application to the northern Hayward fault, California. Bull. Seismol. Soc. Am. 90, 1353–1368.
Waldhauser, F., Ellsworth, W.L., 2002. Fault structure and mechanics of the Hayward Fault, California, from double-difference earthquake locations. J. Geophys. Res. 107. doi:10.1029/2000JB000084.
Wu, Y.M., Chen, Y.G., Shin, T.C., Kuochen, H., Hou, C.S., Hu, J.C., Chang, C.H., Wu, C.F., Teng, T.L., 2006. Coseismic versus interseismic ground deformation, fault structure inversion and segmentation revealed by 2003 Mw6.8 Chengkung earthquake in eastern Taiwan. Geophys. Res. Lett. 33 10.1029/2005GL024.
Yu, S.B., Kuo, L.C., 2001. Present-day crustal motion along the Longitudinal Valley Fault, eastern Taiwan. Tectonophysics 333, 199–217.
Yu, S.B., Liu, C.C., 1989. Fault creep on the central segment of the Longitudinal Valley fault, eastern Taiwan. Proc. Geol. Soc. China 32, 209–231.
Yu, S.B., Jackson, D.D., Yu, G.K., Liu, C.C., 1990. Dislocation model for crustal deformation in the Longitudinal Valley area, eastern Taiwan. Tectonophysics 183, 97–109.
Yu, S.B., Chen, H.Y., Kuo, L.C., 1997. Velocity field of GPS stations in the Taiwan area. Tectonophysics 274, 41–59.